Dalton Transactions

RSC Publishing

PAPER

View Article Online
View Journal

# Asymmetric zinc(II) complexes as functional and structural models for phosphoesterases†

Cite this: DOI: 10.1039/c3dt50514f

Lena J. Daumann, Laurène Marty, Gerhard Schenk and Lawrence R. Gahan*

We report two asymmetric ligands for the generation of structural and functional dinuclear metal complexes as phosphoesterase mimics. Two zinc(II) complexes, $[Zn_2(CH_3\mathbf{L4})(CH_3CO_2)_2]^+$ ($CH_3H\mathbf{L4}$ = 2-(((2-methoxyethyl)(pyridin-2-ylmethyl)amino)methyl)-4-methyl-6-(((pyridin-2-ylmethyl)amino)methyl)-phenol) and $[Zn_2(CH_3\mathbf{L5})(CH_3CO_2)_2]^+$ ($CH_3H\mathbf{L5}$ = 2-(((2-methoxyethyl)(pyridine-2-ylmethyl)amino)-methyl)-4-methyl-6-(((pyridin-2-ylmethyl)(4-vinylbenzyl)amino)methyl)phenol) were synthesized and characterized by X-ray crystallography. The structures showed that the ligands enforce a mixed 6,5-coordinate environment in the solid state. $^1$H-, $^{13}$C- and $^{31}$P-NMR, mass spectrometry and infrared spectroscopy were used to further characterize the compounds in the solid state and in solution. The zinc(II) complexes hydrolyzed the organophosphate substrate bis-(2,4-dinitrophenol)phosphate (BDNPP), the nucleophile proposed to be a terminal water molecule ($pK_a$ 7.2). The ligand $CH_3H\mathbf{L4}$ was immobilised on Merrifield resin and its zinc(II) complex generated. Infrared spectroscopy, microanalysis and XPS measurements confirmed successful immobilisation, with a catalyst loading of ~1.45 mmol g$^{-1}$ resin. The resin bound complex was active towards BDNPP and displayed similar pH dependence to the complex in solution.

Received 26th February 2013,
Accepted 2nd May 2013

DOI: 10.1039/c3dt50514f

www.rsc.org/dalton



## Introduction

In order to generate more structurally comparable biomimetics for dinuclear metallohydrolases much effort has been devoted to the synthesis of asymmetric ligands. It has been proposed that these asymmetric complexes are not only more appropriate functional models for the active site of phosphoesterase enzymes, but also that they exhibit enhanced catalytic rates compared with their symmetric counterparts.[1–3] Ligands used to generate purple acid phosphatase,[1,4–10] phosphoesterase,[11] urease,[12,13] catechol oxidase[14] and manganese catalase biomimetics[15,16] have been reported. Some ligands engender both a hard and a soft coordination site resulting in heterodinuclear complexes as, for example, models for purple acid phosphatase metalloenzymes.[4,7] In other cases the ligands have a structural variation in one arm[4,6,7] whilst in others one donor arm has been omitted,[1,14–16] with the vacant coordination site often found to be occupied by water or solvent molecules in the complex.[15,16]

By careful design the asymmetric ligand can offer both differentiated metal binding sites, and/or sites for further synthetic elaboration. For example, an asymmetric Fe(III)Zn(II) purple acid phosphatase (PAP) model complex with potential for immobilisation on 3-aminopropyl silica has been reported.[17] The immobilised complex exhibited reaction rates toward the hydrolysis of BDNPP similar to those found with the free complex; in addition, the immobilised catalyst was reusable. In addition, a PAP model with pendant olefinic arms suitable for copolymerisation and thus incorporation into a polymer has also been reported.[18] Such biomimetics, and ultimately metalloenzymes, immobilised on inorganic solid supports, have the potential for organophosphate pesticide bioremediation. The immobilisation of complexes on inorganic or organic supports has been extensively explored and modified silica, organic resins such as Tentagel or Merrifield resin and other polymers have served previously as supports.[19,20] Merrifield resin attached complexes have been reported useful for various applications such as Ni(II) catalysed cross coupling reactions,[21] the oxidative DNA cleavage catalysed by an immobilised cyclen Cu(II),[20] Pd(II) catalysed Suzuki–Miyaura cross-coupling reactions,[19] salen Mn(II) complexes for epoxidation reactions,[22] and the Co(II) catalysed polymerisation of vinyl acetate,[23] to list a few examples. The advantage of the immobilised system is that the complex can be easily separated from the reaction mixture and the loaded resin recycled.

*School of Chemistry and Molecular Biosciences, The University of Queensland, Brisbane, QLD 4072, Australia. E-mail: gahan@uq.edu.au*

†Electronic supplementary information (ESI) available: Mass spectra, NMR titrations, IR spectra and additional XPS data can be found in the ESI. CCDC 925903 and 925904. For ESI and crystallographic data in CIF or other electronic format see DOI: 10.1039/c3dt50514f

We have been interested in the glycerophosphodiesterase enzyme (GpdQ) from *Enterobacter aerogenes*. GpdQ is a highly promiscuous dinuclear metallohydrolase with respect to both substrate specificity and metal ion composition; in addition, it is particularly robust suggesting that it may be a promising candidate for bioremedial applications.[24–28] In order to fully study this metalloenzyme we have prepared a number of mimics of its active site structure in order to investigate the mechanism of action with a view to preparing active model systems.[29]

In this work we describe the synthesis and characterisation of two asymmetric ligands 2-(((2-methoxyethyl)(pyridin-2-ylmethyl)-amino)methyl)-4-methyl-6-(((pyridin-2-ylmethyl)amino)methyl)-phenol ($CH_3$H**L4**) and 2-(((2-methoxyethyl)(pyridine-2-ylmethyl)-amino)methyl)-4-methyl-6-(((pyridin-2-ylmethyl)(4-vinylbenzyl)-amino)methyl)phenol ($CH_3$H**L5**) (Chart 1) and their respective zinc(II) complexes as structural and functional models for the enzyme GpdQ. The immobilisation of the complex with $CH_3$H**L4** on Merrifield resin and the activity towards the substrate bis-(2,4-dinitrophenol)phosphate (BDNPP) are reported.

## Materials and methods

### General methods

$^1$H NMR spectra were recorded at room temperature with a 300, 400 or 500 MHz Bruker AV 300/400/500 spectrometer. Chemical shifts are reported in $\delta$ units relative to $CHCl_3$ ($\delta_H$ = 7.24), $CD_3CN$ ($\delta_H$ = 1.93). The following abbreviations were used: s = singlet, d = doublet, t = triplet, dd = doublet of doublet, dt = doublet of triplet, m = multiplet. The software used for data processing was TOPSPIN 2.1. $^{13}$C NMR spectra were recorded at room temperature with a 100 MHz Bruker AV 400/500 spectrometer. Chemical shifts are given in $\delta$ units relative to $CDCl_3$ (central line of triplet: $\delta_C$ = 77.0), d$^4$-MeOD ($\delta_C$ = 49.0), $CD_3CN$ ($\delta_C$ = 1.30), $D_2O$ with 5% dioxane ($\delta_C$ = 67.2). Two-dimensional correlation spectroscopy (COSY), heteronuclear single quantum correlation (HSQC) and heterobinuclear multiple bond connectivity (HMBC) experiments were used to assign each signal in the spectra of the final ligands. $^{31}$P NMR spectra were recorded at room temperature with 85% phosphoric acid as external standard ($\delta_P$ = 0.00). Positive-ion electrospray mass spectrometry was carried out with a Q-Star time-of-flight mass spectrometer, and the data were processed with Bruker Compass Data Analysis 4.0 software. FT-Infrared spectroscopy was carried out with a Perkin Elmer FT-IR Spectrometer SPECTRUM 2000 with a Smiths DuraSamplIR II ATR diamond window. Elemental microanalyses (C, H, N) were performed with a Carlo Erba Elemental Analyser, model NA1500, by Mr George Blazak at the University of Queensland. X-ray photoelectron spectroscopy (XPS) was conducted with Dr Barry Wood at the Centre for Microscopy and Microanalysis, University of Queensland, with a Kratos Axis Ultra photoelectron spectrometer which uses Al $K_\alpha$ (1253.6 eV) X-rays. The software Casa XPS was used for data processing.

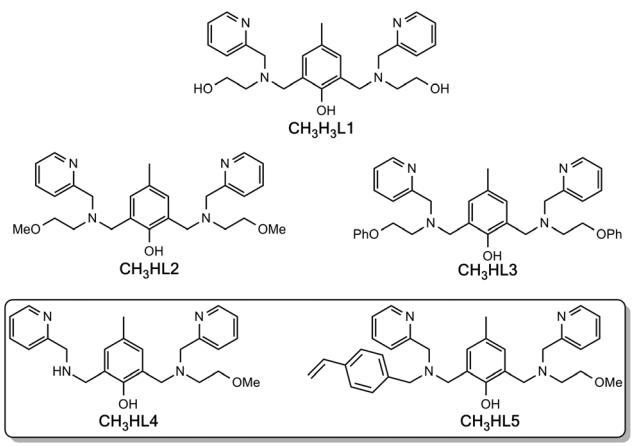


**Chart 1** Ligands reported previously and the two new $CH_3$H**L4** and $CH_3$H**L5** ligands.

### Kinetic studies

Kinetic studies were conducted with bis-(2,4-dinitrophenol)-phosphate (BDNPP) as substrate using a Varian Cary50 Bio UV/Visible spectrophotometer with a Peltier temperature controller and 10 mm quartz cuvettes. The initial-rate method was employed, and assays were measured such that the initial linear portion of the data was used for analysis. Product formation was determined at 25 °C by monitoring the formation of 2,4-dinitrophenol. Throughout the pH range studied (4.75–8.5), the extinction coefficient of this product at 400 nm varies from 7180 at pH 4.5, 10 080 at 5.0; 11 400 at pH 5.5 to 12 000 at 6.0 and 12 100 at pH 6.5–8.5.[30] All assays were measured in 50 : 50 acetonitrile–buffer with the substrate and complex initially dissolved in acetonitrile. The aqueous multicomponent buffer was comprised of 50 mM 2-(*N*-morpholino)-ethanesulfonic acid (MES), 4-(2-hydroxyethyl)-1-piperazineethanesulfonic acid (HEPES), 2-(*N*-cyclohexylamino)ethane sulfonic acid (CHES) and *N*-cyclohexyl-3-aminopropanesulfonic acid (CAPS) with controlled ionic strength ($LiClO_4$) 250 mM. The pH values reported are those of the aqueous component; it should however be noted that the pH of a solution of the buffer was the same within error as a 1 : 1 mixture of buffer and acetonitrile.[31] Assays for pH dependence were 40 μM in complex and 5 mM in BDNPP; for substrate dependence they were 40 μM in complex and 1–11.5 mM in BDNPP. pH-dependence data for monoprotic events were fit to eqn (1).[32]

$$v_0 = \frac{v_{max}}{1 + ([H^+]/K_a)} \quad (1)$$

The data derived from substrate dependence were fit to the Michaelis–Menten eqn (2).[32]

$$v_0 = \frac{v_{max}[S]}{K_M + [S]} \quad (2)$$

Here, $v_0$ is the initial rate, $v_{max}$ is the maximum rate, $K_M$ is the Michaelis constant, and [S] is the substrate concentration.

Complex dependence was measured with a fixed substrate concentration at 5 mM and complex concentrations ranging from 20–120 μM. Background assays were conducted by measuring the autohydrolysis and hydrolysis by two equivalents of zinc(II) acetate and were subtracted from the data. For the kinetic investigation of the immobilised resin, an assay was established which allowed determination of the amount of BDNPP hydrolysed by the resins. In order to obtain initial rates, the absorbance of a solution of multicomponent buffer, acetonitrile and BDNPP was determined ($T = 0$), and then 0.5 mg of resin added. After 15 minutes 1 mL of the suspension was transferred to an Eppendorf tube and centrifuged for 10 seconds; the absorbance of the supernatant was measured again ($T = 15$) and the Abs/min calculated. For every value this was done in triplicate, however, due to swelling properties of the resin and inhomogeneous catalyst loading on the Merrifield beads the errors were larger than for the free complex.

### Crystallographic measurements

Crystallographic data for the complexes were collected at 293(2) K ($[Zn_2(CH_3\mathbf{L4})(CH_3CO_2)_2]PF_6$) and 150 K ($[Zn_2(CH_3\mathbf{L5})(CH_3CO_2)_2]BPh_4$) with an Oxford Diffraction Gemini Ultra dual source (Mo and Cu) CCD diffractometer, for the former using Mo ($\lambda_{K\alpha}$ = 0.71073 Å) and the latter using Cu ($\lambda_{K\alpha}$ = 1.5418 Å) radiation. The structures were solved by direct methods (SIR-92)[33] and refined (SHELXL 97)[34] by full matrix least squares methods based on $F^2$.[35] These programs were accessed through the WINGX 1.70.01 crystallographic collective package.[36] All non-hydrogen atoms were refined anisotropically unless they were disordered. Hydrogen atoms were fixed geometrically and were not refined. X-ray data of the published structures were deposited with the Cambridge Crystallographic Data Centre CCDC 925903 and 925904.

### Ligand syntheses

3-(Chloromethyl)-2-hydroxy-5-methylbenzaldehyde and 2-methoxy-*N*-(pyridin-2-ylmethyl)aminoethanol were prepared following previously published procedures.[29,37] Merrifield resin (1% crosslinked, 3.5 mmol $g^{-1}$ Cl) was obtained from Aldrich Chemical Company (microanalysis found C 80.18, H 6.64%).

**Synthesis of 2-(((2-methoxyethyl)(pyridin-2-ylmethyl)amino)methyl)-4-methyl-6-(((pyridin-2-ylmethyl)amino)methyl)-phenol ($CH_3$HL4).** Triethylamine (2.6 mL) was added drop wise to a mixture of 3-(chloromethyl)-2-hydroxy-5-methylbenzaldehyde (1.0 g, 6.0 mmol) and 2-methoxy-*N*-(pyridin-2-ylmethyl)ethanamine (1.0 g, 6.0 mmol) in tetrahydrofuran (45 mL) at room temperature and the mixture stirred for 24 hours. After filtration and concentration *in vacuo* the residue was taken up in water (30 mL) and extracted with dichloromethane (3 × 30 mL). The combined organic extracts were dried over $Na_2SO_4$ and concentrated *in vacuo* to yield 1.69 g (89%) of crude 2-hydroxy-3-(((2-methoxyethyl)(pyridin-2-ylmethyl)amino)methyl)-5-methylbenzaldehyde as an orange oil which was used in the next step without further purification. The 2-hydroxy-3-(((2-methoxyethyl)(pyridin-2-ylmethyl)amino)methyl)-5-methylbenzaldehyde (1.69 g, 5.37 mmol) was dissolved in methanol (50 mL) and 2-aminomethylpyridine (0.58 g, 5.37 mmol) in methanol (25 mL) added drop wise at room temperature. The resulting mixture was stirred at 50 °C for two hours, the mixture subsequently cooled to 0 °C and sodium borohydride (0.72 g, 19.0 mmol) added in small portions. After heating to reflux for 3 hours the mixture was concentrated *in vacuo*, taken up in acidified water (100 mL, pH 2) and extracted with dichloromethane (3 × 35 mL). The combined organic extracts were washed with saturated $NaHCO_3$ solution (3 × 50 mL) and dried over $Na_2SO_4$. After removal of the solvent *in vacuo* the crude ligand (1.53 g, 70%) was purified with flash column chromatography (EtOAc until the first band was eluted, MeOH–EtOAc 9 : 1, $FeCl_3$ stain, $R_f$ = 0.48 in EtOAc) to yield 900 mg (41%) of the ligand as a yellow oil. $^1$H NMR ($CDCl_3$, 500.13 MHz) $\delta$ 2.20 (s, 3H, arCC$H_3$); 2.76 (t, 2H, NC$H_2$CH$_2$, $J$ = 5.5 Hz); 3.26 (s, 3H, OC$H_3$); 3.50 (t, 2H, NCH$_2$C$H_2$, $J$ = 5.5 Hz); 3.77 (s, 2H, arCC$H_2$N); 3.85 (s, 2H, arCC$H_2$NH); 3.92 (s, 2H, NC$H_2$py); 3.96 (s, 2H, NHC$H_2$py); 6.78 (d, 1H, arC$H$, $J$ = 1.8 Hz); 6.92 (d, 1H, arC$H$, $J$ = 1.8 Hz); 7.13 (qd, 2H, py$H$, $J$ = 7.4, 1.2 Hz); 7.34 (dd, 2H, py$H$, $J$ = 5.1, 1.5 Hz); 7.62 (tt, 2H, py$H$, $J$ = 7.6, 1.9 Hz); 8.51 (ddt, 2H, py$H$, $J$ = 6.6, 1.7, 0.9 Hz). $^{13}$C NMR ($CDCl_3$, 100.62 MHz) $\delta$ 20.4 (arC$C$H$_3$); 49.2 (N$C$H$_2$py); 52.6 (N$C$H$_2$CH$_2$); 53.7 (NH$C$H$_2$py); 56.9 (arC$C$H$_2$N); 58.6 (O$C$H$_3$); 60.0 (arC$C$H$_2$NH); 70.1 (NCH$_2$$C$H$_2$); 122.0 (py$C$H); 122.2 (py$C$H); 122.3 (py$C$H); 122.4 (ar$C$); 123.4 (py$C$H); 124.4 (ar$C$); 127.8 (ar$C$CH$_3$); 129.2 (ar$C$H); 129.7 (ar$C$H); 136.5 (py$C$H); 136.6 (py$C$H); 148.9 (py$C$H); 149.0 (py$C$H); 153.5 (ar$C$OH); 158.0 (py$C$CH$_2$); 158.6 (py$C$CH$_2$). FT-IR spectroscopy ($\nu$, $cm^{-1}$) 3402.3 (m, O–H str); 2917.2, 2818.5 (m, C–H str); 1108.4 (m, C–O str); 862.5 (w, ar-H); 755.2 (s, py-H). ESI mass spectrometry (methanol) $m/z$ 407.23 $[C_{24}H_{30}N_4O_2 + H]^+$.

**Synthesis of 2-(((2-methoxyethyl)(pyridine-2-ylmethyl)-amino)methyl)-4-methyl-6-(((pyridin-2-ylmethyl)(4-vinylbenzyl)-amino)methyl)phenol ($CH_3$HL5).** $CH_3$H**L4** (500 mg, 1.2 mmol) and vinylbenzyl chloride (0.174 mL, 1.1 mmol) were stirred with dry powdered potassium carbonate (0.256 g, 1.9 mmol) in acetonitrile (5 mL) at room temperature for two days. After this time the mixture was filtered and concentrated *in vacuo*. The crude residue was purified by flash column chromatography (EtOAc–MeOH 5 : 2) and $CH_3$H**L5** obtained as orange oil (yield: 38%, 0.24 g). $^1$H NMR ($CDCl_3$, 500.13 MHz) $\delta$ 2.24 (s, 3H, arCC$H_3$); 2.77 (t, 2H, NC$H_2$CH$_2$, $J$ = 5.7 Hz); 3.27 (s, 3H, OC$H_3$); 3.52 (t, 2H, NCH$_2$C$H_2$, $J$ = 5.7 Hz); 3.65 (s, 2H, C$H_2$); 3.71 (s, 2H, C$H_2$); 3.77 (s, 2H, C$H_2$); 3.79 (s, 2H, C$H_2$); 3.86 (s, 2H, C$H_2$); 5.19 (dd, 1H, CH=C$H_2$ *cis*, $J$ = 10.9, 0.6 Hz); 5.69 (dd, 1H, CH=C$H_2$ *trans*, $J$ = 17.6, 0.8 Hz); 6.67 (dd, 1H, C$H$=CH$_2$, $J$ = 17.6, 10.9 Hz); 6.89 (d, 1H, arC$H$, $J$ = 1.7 Hz); 7.03 (d, 1H, arC$H$, $J$ = 1.8 Hz); 7.13 (m, 2H, pyC$H$, $J$ = 6.4, 0.9 Hz); 7.34 (s, 4H, vinylbenzyl$H$); 7.43 (d, 1H, pyC$H$, $J$ = 7.8 Hz); 7.51 (d, 1H, pyC$H$, $J$ = 7.8 Hz); 7.62 (m, 2H, pyC$H$, $J$ = 7.7, 1.8 Hz); 8.51 (m, 2H, pyCH, $J$ = 0.9 Hz). $^{13}$C NMR ($CDCl_3$, 100.62 MHz) $\delta$ 20.6 (arC$C$H$_3$); 52.9 (N$C$H$_2$CH$_2$); 53.8 (C$H_2$); 55.7 (C$H_2$); 57.9 (C$H_2$); 58.6 (O$C$H$_3$); 59.6 (C$H_2$); 60.4 (C$H_2$); 70.4 (NCH$_2$$C$H$_2$); 113.4 (CH=$C$H$_2$); 121.8 (py$C$H); 122.0 (py$C$H); 122.9 (py$C$H); 123.2 (py$C$H); 123.9 (ar$C$-CH=CH$_2$); 126.1 (vinylbenzyl ar$C$H); 127.5

(ar*C*$CH_3$); 129.0 (ar*C*H); 129.1 (vinylbenzyl ar*CH*); 129.3 (ar*CH*); 136.4 (py*C*H); 136.5 (py*C*H); 136.6 (*C*H═$CH_2$); 138.5 (arC); 148.8 (py*C*H); 148.9 (py*C*H); 153.5 (ar*C*OH); 158.0 (py*C*$CH_2$); 158.6 (py*C*$CH_2$). FT-IR spectroscopy ($\nu$, $cm^{-1}$) 2918.3, 2815.5 (m, C–H str); 1108.5 (m, C–O str); 860.9 (w, ar-H); 755.4 (s, py-H). ESI mass spectrometry (methanol) *m*/*z* 523.20 $[C_{33}H_{38}N_4O_2 + H]^+$.

**Synthesis of $[Zn_2(CH_3L4)(CH_3CO_2)_2](PF_6)$.** $CH_3$H**L4** (80 mg, 0.2 mmol) and zinc(II) acetate dihydrate (86 mg, 0.4 mmol) were combined in methanol (5 mL) and refluxed for 30 min. After the solution was cooled to room temperature sodium hexafluorophosphate (65 mg, 0.4 mmol) was added, the pale yellow solution filtered and left to evaporate. The white crystals which formed after 3 days were collected and dried in air (85 mg, 54.8%). ESI mass spectrometry (methanol) *m*/*z*: 655.11 $[C_{28}H_{35}N_4O_6Zn_2]^+$, 595.06 $[C_{26}H_{31}N_4O_4Zn_2]^+$; (acetonitrile) *m*/*z* = 749.1, calc. *m*/*z* 749.17 (100%), 748.17 (79.2%), $[C_{60}H_{88}N_{10}O_{18}Zn_4]^{2+}$. FT-IR spectroscopy ($\nu$, $cm^{-1}$) 3306.9 (w, N–H str); 2925.3 (w, C–H str); 1596.3 (s, bridging acetate antisym. str); 1421.6 (s, bridging acetate sym. str); 832.3 (s, P–F str); 767.7, 663.1 (m, pyH def); 555.6 (m, P–F). Microanalysis Anal calc. for $C_{28}H_{38}N_4O_6Zn_2PF_6$ C 41.29, H 4.24, N 7.13; found: C 41.21, H 4.25, N 6.72%. $^1$H NMR ($CD_3CN$, 500.13 MHz); $\delta$ 1.97 (s, 6H, acetate$CH_3$); 2.55 (m, 2H, NC$H_2CH_2$); 2.75 (m, 1H, $NCH_2CH_2$); 2.82 (d, 1H $NCH_2CH_2$, *J* = 11.1 Hz); 3.04 (s, 3H, O$CH_3$); 3.65 (d, 1H, ar$CH_2$N, *J* = 12.2 Hz); 3.79 (d, 1H, N$CH_2$py, *J* = 11.4 Hz); 3.85 (d, 1H, N$CH_2$py, *J* = 15.0 Hz); 3.99 (t, 1H, ar$CH_2$N, *J* = 12.8 Hz); 4.13 (t, 1H, N$CH_2$py, *J* = 11.6 Hz); 4.21 (dd, 1H, ar$CH_2$N, *J* = 12.1, 5.1 Hz); 4.31 (d, 1H, N$CH_2$py, *J* = 15.2 Hz); 4.35 (d, 1H, ar$CH_2$N, *J* = 12.3 Hz); 6.94 (s, 1H, ar*H*); 6.97 (s, 1H, ar*H*); 7.40–7.35 (m, 4H, py*H*); 7.98 (mc, 2H, py*H*, *J* = 7.7, 0.8 Hz); 8.60 (d, 1H, py*H*, *J* = 4.8 Hz); 8.77 (d, 1H, py*H*, *J* = 4.7 Hz). $^{13}$C NMR ($CD_3CN$, 100.62 MHz); 20.3 ($CH_3$); 24.3 (acetate$CH_3$); 51.5 (ar$CH_2$N); 52.8 ($NCH_2$py); 55.1 ($CH_2CH_2$); 59.1 (O$CH_3$); 61.9 (ar$CH_2$N); 69.6 ($CH_2CH_2$); 124.2 (py*C*H); 125.0 (py*C*H); 125.1 (py*C*H); 125.3 (py*C*H); 125.8 (ar*C*); 126.4 (arC); 126.4 (ar*C*$CH_3$); 132.2 (ar*C*H); 132.8 (arCH); 140.8 (py*C*H); 141.0 (py*C*H); 148.6 (py*C*H); 148.7 (pyCH); 155.8 (py*C*); 161.1 (ar*C*O); 168.4 (*C*$O_2^-$).

**Synthesis of $[Zn_2(CH_3L5)(CH_3CO_2)_2](PF_6)\cdot$MeOH.** $CH_3$H**L5** (50 mg, 0.09 mmol) and zinc(II) acetate dihydrate (42 mg, 0.19 mmol) were combined in methanol (5 mL) and refluxed for 30 min. After cooling to room temperature, sodium hexafluorophosphate (48 mg, 0.29 mmol) was added, the pale yellow solution filtered and left to evaporate. After 3 days the resulting white powder was collected and dried in air (29 mg, 37%). Crystals suitable for X-ray structure analysis were obtained as follows: $CH_3$H**L5** (30 mg, 0.05 mmol) and zinc(II) acetate dihydrate (25 mg, 0.11 mmol) were combined in methanol (3 mL) and refluxed for 30 min, and after cooling to room temperature sodium tetraphenylborate (59 mg, 0.17 mmol) was added and the pale yellow solution filtered and left to evaporate. The white powder was taken up in acetone/isopropanol and layered with hexane which yielded colourless crystals, desiccating readily upon removal from the solvent. X-ray structure analysis was thus conducted at 150 K. Further analysis was done with the hexafluorophosphate derivative. ESI mass spectrometry (methanol) *m*/*z* = 751.1 (100%), 749.1 (95%) calc. for $[C_{35}H_{47}N_4O_6Zn_2]^+$ *m*/*z* = 749.2 (100%), 751.2 (96.1%); (acetonitrile) *m*/*z* = 851.3, calc. 851.23 (100%), 849.23 (85.5%) $[C_{41}H_{49}N_6O_6Zn_2]^+$; *m*/*z* = 769.1, calc. 769.17 (100%), 767.18 (87%), $[C_{37}H_{43}N_4O_6Zn_2]^+$; *m*/*z* = 723.1, calc. 721.17 (100%), 732.17 (96.6%), $[C_{33}H_{43}N_4O_6Zn_2]^+$), *m*/*z* = 653.1, calc. *m*/*z* 653.11 (100%), 655.11 (96.2%), $[C_{28}H_{35}N_4O_6Zn_2]^+$. FT-IR spectroscopy ($\nu$, $cm^{-1}$) 2926.6, 2856.4 (w, C–H str); 1597.8 (s, bridging acetate antisym. str); 1431.4 (s, bridging acetate sym. str); 832.1 (s, P–F str); 764.6, 728.5 (m, pyH def); 555.3 (m, P–F). Microanalysis Anal calc. for $C_{38}H_{48}N_4O_7Zn_2PF_6$ C 48.12, H 5.10, N 5.91; found: C 48.19, H 4.71, N 5.36%. $^1$H NMR ($CD_3CN$, 500.13 MHz) $\delta$ 1.94 (s, 6H, C$H_3CO_2^-$); 2.14 (s, 3H, ar$CH_3$); 2.50–2.56 (m, 2H, NC$H_2CH_2$); 2.84–2.90 (m, 2H, $NCH_2CH_2$); 3.03 (s, 3H, O$CH_3$); 3.57 (d, 1H, ar$CH_2$N, *J* = 12.6 Hz); 3.64 (d, 1H, N$CH_2$py, *J* = 12.1 Hz); 3.71–3.91 (m, 5H, $CH_2$); 4.15 (d, 1H, ar$CH_2$N, *J* = 12.5); 4.21–4.27 (m, 2H, $CH_2$); 5.20 (d, 1H, CH═$CH_2$, $J_{cis}$ = 10.9 Hz); 5.25 (dd, 1H, CH═$CH_2$, $J_{cis}$ = 11.0, 0.5 Hz, second isomer); 5.69 (d, 1H, CH═$CH_2$, $J_{trans}$ = 17.6 Hz); 5.81 (d, 1H, CH═$CH_2$, $J_{trans}$ = 17.6 Hz, second isomer); 6.62 (dd, 1H, C*H*═$CH_2$, *J* = 17.7, 10.9, 0.8 Hz); 6.71 (dd, 1H, C*H*═$CH_2$, *J* = 17.7, 10.9 Hz, second isomer); 6.81 (d, 2H, ar*CH*, *J* = 1.8 Hz); 6.89 (d, 2H, ar*CH*, *J* = 1.8 Hz); 6.95 (s, 2H, ar*CH*); 7.10–7.53 (m, 4H, py*CH*); 7.91 (m, 2H, py*CH*, *J* = 7.8, 1.6 Hz); 8.70 (m, 2H, py*CH*). $^{13}$C NMR ($CD_3CN$, 100.62 MHz) $\delta$ 20.2 (ar*C*$CH_3$); 23.1 ($CH_3CO_2^-$); 54.7 ($CH_2$); 58.6 (O$CH_3$); 59.1, 59.5, 60.8, 61.2, 61.3, 69.3 ($CH_2$); 114.9 (CH═$CH_2$); 115.2 (CH═$CH_2$, second isomer); 124.0, 124.3, 124.7, 125.0, 125.1 (py*C*H); 125.2, 125.3 ($C_{quart}$); 126.8, 126.9 (CH); 127.0, 127.3, 131.6 ($C_{quart}$), 132.8, 133.0 (CH); 133.2 (CH); 133.6 (CH); 133.7 ($C_{quart}$); 137.1 (*C*H═$CH_2$); 138.5 (arC); 140.8, 141.3, 141.5, 148.2, 148.5, 149.8 (CH); 155.8, 156.5, 160.8, 161.4 ($C_{quart}$), 179.0 ($CH_3CO_2^-$).

**Immobilisation of $CH_3$H**L4** on Merrifield resin (M-$CH_3$H**L4**).** To Merrifield resin (1% crosslinked, 3.5 mmol $g^{-1}$ Cl, 500 mg) in acetonitrile (10 mL) was added $CH_3$H**L4** (320 mg, 0.78 mmol) and potassium carbonate (250 mg) and the mixture stirred for 10 days. After this time the orange beads of the resin were dried on a sintered glass funnel (the filtrate was collected to recover any unbound ligand) and washed with water (20 mL) and methanol (20 mL). The resin was further dried under high vacuum to yield 646 mg of M-$CH_3$H**L4**. 26 mg of ligand were recovered from the filtrate. Total loading 1.45 mmol ligand $g^{-1}$ resin. FT-IR spectroscopy ($\nu$, $cm^{-1}$) 3352.3 (b, O–H str); 3024.5, 2921.7 (w, C–H str); 1110.0 (m, C–O–C str); 814.4, 756.4, 699.4 (m, Ar-H/Py-H str). Microanalysis found C 77.39, H 7.22, N 4.86%.

**Synthesis of the immobilised zinc(II) complex M-$[Zn_2(CH_3L4)(CH_3COO)_2]$.** To M-$CH_3$H**L4** (400 mg) in methanol (10 mL) was added zinc(II) acetate dihydrate (400 mg) and the mixture refluxed for 30 minutes and then stirred for 24 h. Subsequently the resin was dried and washed with water (10 mL) and methanol (20 mL) to yield 505 mg of the immobilised complex M-$[Zn_2(CH_3L4)(CH_3COO)_2]$. FT-IR spectroscopy ($\nu$, $cm^{-1}$) 3410.1 (b, O–H str); 3025.4, 2923.5 (w, C–H str); 1596.1

(s, bridging acetate antisym. str); 1420.5 (s, bridging acetate sym. str); 808.9, 760.9, 700.1, 664.3 (m, Ar-H/Py-H str). Microanalysis found C 64.42, H 6.18, N 3.58%. The resin was further characterized with XPS.

## Results and discussion

### Ligand nomenclature

The nomenclature employed for these types of ligands ($CH_3H_3$**L1**, $CH_3H$**L2** and $CH_3H$**L3**, Chart 1) has been described previously;[29] the designations **L4** and **L5** follow this previous nomenclature. In general, the nomenclature employed for the ligands denotes the number of labile protons upon complexation and the substituent on the *para*-position of the phenoxide. Hence, $CH_3H$**L4** and $CH_3H$**L5** have the same phenolate backbone with a methyl group in *para* position of the phenolic oxygen and have one potential site for deprotonation, the phenolic –OH; complexation as $CH_3$**L4**$^-$ and $CH_3$**L5**$^-$ implies a single deprotonation.

### Ligand and complex synthesis

$CH_3H$**L4** ligand synthesis was achieved using a protocol similar to that previously published.[38] Addition of 2-methoxy-*N*-(pyridin-2-ylmethyl)aminoethanol to the 3-(chloromethyl)-2-hydroxy-5-methylbenzaldehyde precursor, subsequent Schiff base condensation with 2-aminomethylpyridine and reduction with sodium borohydride gave the desired ligand $CH_3H$**L4** as a yellow oil in moderate yield. Treatment of $CH_3H$**L4** with vinyl benzyl chloride in the presence of potassium carbonate resulted in the ligand $CH_3H$**L5**. For the dizinc(II) complex with $CH_3H$**L4**, crystals suitable for X-ray crystallography were obtained after multiple crystallisations using ether diffusion into a methanolic solution of the complex. Crystals of $[Zn_2(CH_3$**L5**$)(CH_3COO)_2]BPh_4$ were obtained after slow diffusion (3 weeks) of hexane into an acetone solution of the complex. The crystals desiccated upon removal from the mother liquor, requiring low temperature during X-ray structure analysis. The remaining analysis of this complex was undertaken with the $[Zn_2(CH_3$**L5**$)(CH_3COO)_2]PF_6$ derivative.

### Crystal structures

Both dizinc(II) complexes crystallised in the triclinic space group $P\bar{1}$. The zinc complex with $CH_3$**L4**$^-$ crystallised as an asymmetric complex with one six-coordinate Zn(II) and one Zn(II) in a five-coordinate (distorted trigonal bipyramidal) environment (Fig. 1). Two $\mu_2$-$CH_3COO$-$\kappa^2O{:}O'$ anions but no additional water or solvent molecules are bound to the complex in the solid state. The crystal structure shows the presence of two isomers, one present as a minor component in one of the two asymmetric units. In the major isomer, the pyridine nitrogens are *trans* (*anti*) to each other while in the minor isomer the pyridines are *cis* (*syn*) in respect of the phenolic oxygen.[39] The ORTEP[40] representation of the asymmetric unit which contains two $[Zn_2(CH_3$**L4**$)(CH_3COO)_2]PF_6$ complex entities is shown (Fig. 1). The $[Zn_2(CH_3$**L5**$)(CH_3COO)_2]BPh_4$ complex crystallized with one Zn(II) ion six coordinate and the other in a five coordinate environment (Fig. 1). The vinylbenzyl group is arranged in such a way that it shields one site on the second Zn(II) ion leaving this site almost square pyramidal. Crystallographic data and selected bond lengths and angles are displayed in Tables 1 and 2, respectively.

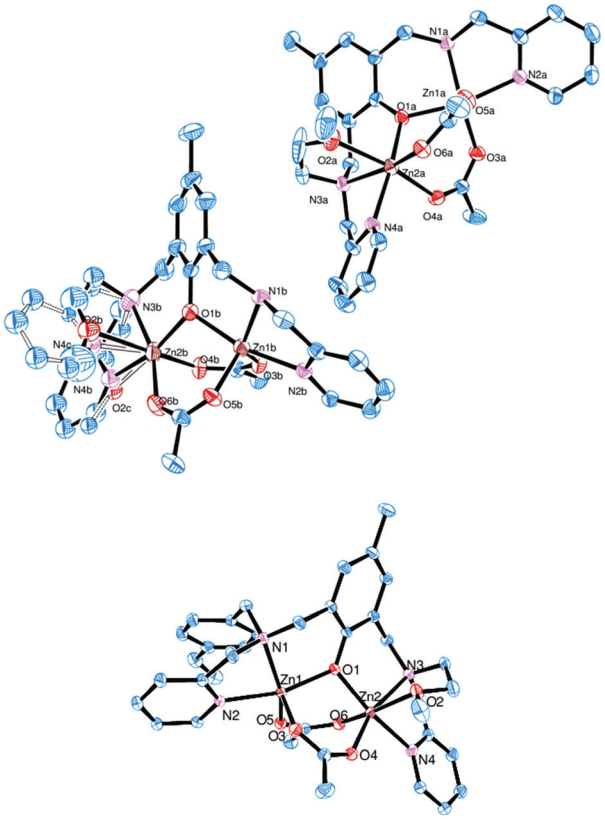


**Fig. 1** ORTEP plots (25%) of the two asymmetric complexes. Top: the two molecules in the asymmetric unit of $[Zn_2(CH_3$**L4**$)$-$(CH_3COO)_2]PF_6$, with the pyridine and methyl-ether arm positions of the minor isomer represented in dashed bonds. Bottom: $[Zn_2(CH_3$**L5**$)$-$(CH_3COO)_2]BPh_4$. Counter ions, solvent molecules and hydrogen atom are omitted for clarity.

The comparison of the bond lengths to the symmetrical counterpart $[Zn_2(CH_3$**L2**$)(CH_3COO)_2]PF_6$[29] show that the $O_{Phenol}$–Zn bonds are similar with a mean of 2.024 Å for the asymmetric and 2.015 Å for the symmetric counterpart. The methyl ether distance is shorter (2.320 Å) than in the symmetric complex (mean 2.432 Å). The $N_{tert}$–Zn (2.124 Å) and $N_{py}$–Zn (2.150 Å) distances are similar to the corresponding distances in $[Zn_2(CH_3$**L2**$)(CH_3COO)_2]PF_6$ (2.186 and 2.1355 Å). The $O_{acetate}$–Zn bond lengths in $[Zn_2(CH_3$**L4**$)(CH_3COO)_2]PF_6$ vary from 1.971–2.058 Å while those from $[Zn_2(CH_3$**L2**$)$-$(CH_3COO)_2]PF_6$ encompass a range from 1.992 to 2.076 Å. The Zn–$O_{Phenol}$–Zn angle is reduced to 108.17° in the asymmetric complex (109.70° with the $CH_3H$**L2** ligand). Zn–Zn distances are as well slightly reduced in the asymmetric complex (3.222, 3.271 Å), as opposed to 3.296 Å in the symmetric counterpart.

The ligands create a geometry which make the zinc complexes appropriate structural mimics of phosphoesterase enzymes such as GpdQ. A close up view of the first

**Table 1** Crystallographic data for $[Zn_2(CH_3\mathbf{L4})(CH_3COO)_2]PF_6$ and $[Zn_2(CH_3\mathbf{L5})(CH_3COO)_2]BPh_4$

| | $[Zn_2(CH_3\mathbf{L4})(CH_3COO)_2]PF_6$ | $[Zn_2(CH_3\mathbf{L5})(CH_3COO)_2]BPh_4$ |
|---|---|---|
| Empirical formula | $C_{28}H_{35}N_4O_6Zn_2$, $P_1F_6$ | $C_{37}H_{39}N_4O_6Zn_2$, $C_{24}H_{20}B$, $C_3H_8O$ |
| Formula weight | 799.31 | 1145.77 |
| Temperature [K] | 293(2) | 150(2) |
| Wavelength [Å] | 0.71073 ($MoK_\alpha$) | 1.5418 ($CuK_\alpha$) |
| Crystal system | Triclinic | Triclinic |
| Space group | $P\bar{1}$ | $P\bar{1}$ |
| $a$ [Å] | 13.137(5) | 13.3209(6) |
| $b$ [Å] | 13.669(6) | 15.0129(7) |
| $c$ [Å] | 20.822(8) | 16.4893(6) |
| $\alpha$ [°] | 85.047(3) | 91.810(3) |
| $\beta$ [°] | 85.468(3) | 108.350(4) |
| $\gamma$ [°] | 66.511(4) | 110.363(4) |
| Volume [Å$^3$] | 3412(2) | 2897.2(2) |
| $Z$ | 4 | 2 |
| $\rho$ [mg m$^{-3}$] | 1.556 | 1.313 |
| $\mu$ [mm$^{-1}$] | 1.530 | 1.466 |
| $F(000)$ | 1632 | 1199.8 |
| $\Theta$ range for data collection [°] | 1.63 to 24.14 | 2.86–61.63 |
| Reflections collected | 33 208 | 26 492 |
| Independent reflections ($R_{int}$) | 10 796 (0.0290) | 8953 (0.0277) |
| GOOF on $F^2$ | 1.032 | 1.035 |
| Final $R$ indices | $R_1$ = 0.0661, | $R_1$ = 0.0480, |
| [$I > 2\sigma(I)$] | w$R_2$ = 0.1831 | w$R_2$ = 0.1321 |
| $R$ indices (all data) | $R_1$ = 0.0779, | $R_1$ = 0.0557, |
| | w$R_2$ = 0.1940 | w$R_2$ = 0.1401 |
| CCDC number | 925903 | 925904 |

**Table 2** Selected bond lengths [Å] and angles [°] for $[Zn_2(CH_3\mathbf{L4})(CH_3COO)_2]PF_6$ and $[Zn_2(CH_3\mathbf{L5})(CH_3COO)_2]BPh_4$

| | [$[Zn_2(CH_3\mathbf{L4})(CH_3COO)_2]PF_6$ [a] | $[Zn_2(CH_3\mathbf{L5})(CH_3COO)_2]BPh_4$ |
|---|---|---|
| N1–Zn1 | 2.133(5) | 2.192(3) |
| N2–Zn1 | 2.121(4) | 2.108(3) |
| N3–Zn2 | 2.182(4) | 2.184(3) |
| N4–Zn2 | 2.121(4) | 2.131(3) |
| O1–Zn1 | 2.026(4) | 2.016(2) |
| O1–Zn2 | 2.014(4) | 2.014(2) |
| O2–Zn2 | 2.320(4) | 2.370(2) |
| O3–Zn1 | 1.984(4) | 2.020(2) |
| O4–Zn2 | 2.112(4) | 2.029(2) |
| O5–Zn1 | 1.998 (4) | 1.986(2) |
| O6–Zn2 | 2.015(4) | 2.072(2) |
| Zn1–O1–Zn2 | 108.17(16) | 106.98(9) |
| Zn1–Zn2 | 3.2714(12) | 3.2391(6) |

[a] Only the bond lengths and angles of the zinc complex labeled with 'a' (*e.g.* Zn1a) are displayed.

coordination sphere of the two Zn(II) ions in the complexes is displayed in Fig. 2 along with the first coordination sphere donor atoms in GpdQ.[27,28] While the acetate ligands do not accurately mimic the bridging water molecules, the general structure, geometry and donor-atoms of GpdQ are reproduced well in the crystal structures.

## Infrared spectroscopy

The $[Zn_2(CH_3\mathbf{L4})(CH_3COO)_2]PF_6$ complex exhibited stretches typical for bridging acetate (1596 and 1422 cm$^{-1}$, $\nu_{asym}$ and $\nu_{sym}$, respectively)[41] and for the $PF_6^-$ counter ion (832, 555 cm$^{-1}$) in addition to the C–O stretching vibration of the methyl ether at 1022 cm$^{-1}$ and the N–H stretch at 3307 cm$^{-1}$. For the $[Zn_2(CH_3\mathbf{L5})(CH_3COO)_2]PF_6$ complex the stretches at 1594 and 1429 cm$^{-1}$ also suggest the presence of bidentate bridging acetate.[41] Moreover, C–H (2925, 2842 cm$^{-1}$), C–O (1022 cm$^{-1}$) and bands typical for aromatic functionalities (766, 662 cm$^{-1}$) are similar to those observed for the complex $[Zn_2(CH_3\mathbf{L4})(CH_3COO)_2]PF_6$ (C–H 2925 cm$^{-1}$, aromatic 768 and 663 cm$^{-1}$). It can thus be assumed that a similar coordination environment with two bridging acetates for $[Zn_2(CH_3\mathbf{L5})(CH_3COO)_2]PF_6$ is found in the solid state.

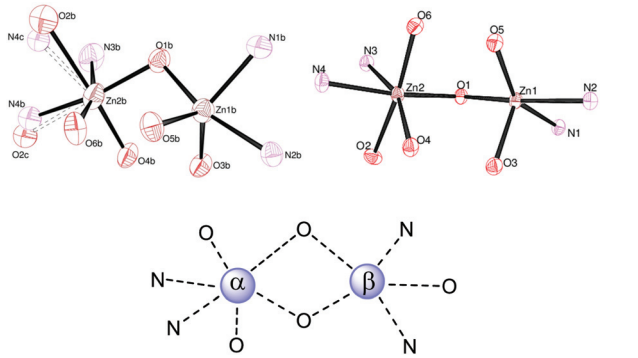


**Fig. 2** First coordination sphere of the two Zn(II) ions in the $[Zn_2(CH_3\mathbf{L4})(CH_3COO)_2]PF_6$ complex (top left), $[Zn_2(CH_3\mathbf{L5})(CH_3COO)_2]BPh_4$ (top right) and in GpdQ (below).

## Mass spectrometry

The electrospray mass spectra of the two zinc complexes were recorded in MeOH and MeCN. The spectrum of $[Zn_2(CH_3\mathbf{L4})(CH_3COO)_2]PF_6$ measured in MeOH is displayed in Fig. S1a† and shows a peak at $m/z$ 655.1 (100%) (calc. $m/z$ = 653.11 (100%), 655.11 (96.2%), $[C_{28}H_{35}N_4O_6Zn_2]^+$) corresponding to one negatively charged ligand, two Zn(II) ions and two acetates. The major ion peak at $m/z$ 641.1 is assigned to $[Zn_2(CH_3\mathbf{L4})(CH_3COO)(HCOO)]^+$ (calc. $m/z$ = 641.1 (100%), 639.1 (98.7%), 637.1 (81.8%), $[C_{27}H_{33}N_4O_6Zn_2]^+$).

The spectrum recorded in MeCN showed multiple doubly charged species, the major ion peak at $m/z$ 749.1 is assigned to a complex with two $CH_3\mathbf{L4}^-$, four Zn(II), four acetates, six water molecules and two MeCN molecules (calc. $m/z$ 749.17 (100%), 748.17 (79.2%), $[C_{60}H_{88}N_{10}O_{18}Zn_4]^{2+}$, Fig. S1b†).

The major ion of the $[Zn_2(CH_3\mathbf{L5})(CH_3COO)_2]PF_6$ complex measured in MeOH corresponds to a $[Zn_2(CH_3\mathbf{L5})(MeO)_2(H_2O)_2]^+$ species (calc. for $C_{35}H_{47}N_4O_6Zn_2^+$ $m/z$ = 749.2 (100%), 751.2 (96.1%), found $m/z$ = 751.1 (100%), 749.1 (95%), Fig. S2a†). Higher molecular weight species with $m/z$ > 800 are also found and are most likely due to coordination of additional solvent and anionic components. A large mass peak due to free ligand is also found at $m/z$ = 523.2 ($CH_3H\mathbf{L5}$ + H). The mass spectrum for $[Zn_2(CH_3\mathbf{L5})(CH_3COO)_2]PF_6$ in MeCN shows at least four major species (Fig. S2b†): (i) observed $m/z$ = 851.3 assigned to $[Zn_2(CH_3\mathbf{L5})(CH_3COO)_2(MeCN)_2]^+$ (calc. $m/z$ = 851.23 (100%), 849.23 (85.5%), $[C_{41}H_{49}N_6O_6Zn_2]^+$); (ii)

observed $m/z$ = 769.1 corresponds to a $[Zn_2(CH_3\mathbf{L5})(CH_3COO)_2]^+$ species (calc. 769.17 (100%), 767.18 (87%), $[C_{37}H_{43}N_4O_6Zn_2]^+$; (iii) a peak at $m/z$ = 723.1 is due to the loss of acetate and coordination of water (calc. $m/z$ = 721.17 (100%), 732.17 (96.6%), $[C_{33}H_{43}N_4O_6Zn_2]^+$), and (iv) the peak at 653.1 can be attributed to the loss of the vinylbenzyl group (calc. $m/z$ 653.11 (100%), 655.11 (96.2%), $[C_{28}H_{35}N_4O_6Zn_2]^+$).

To investigate relevant species occurring during phosphate ester hydrolysis, the mass spectra were measured in MeCN in the presence of diphenyl phosphate (DPP). The $[Zn_2(CH_3\mathbf{L4})(CH_3COO)_2]PF_6$ complex loses acetate ligands under mass spectral conditions and forms, even in the presence of only one equivalent DPP (Fig. S3a†), a complex with two DPP bound (100%), illustrating the high affinity of this complex for phosphoester substrates. In addition, a small peak (~25%) arising from complex with one DPP, one hydroxide and an acetonitrile solvent molecule is observed.

For $[Zn_2(CH_3\mathbf{L5})(CH_3COO)_2]PF_6$ the mass spectrum in the presence of one equivalent DPP is different (Fig. S3b†). The base peak arises from a species with one DPP, a hydroxide and MeCN; two peaks complexes arising from intact complex with two acetates (29%) or two DPP molecules (47%) bound are present. It is proposed that under the conditions of the mass spectral measurements $[Zn_2(CH_3\mathbf{L4})(CH_3COO)_2]PF_6$ has a high affinity for diphenylphosphate (Fig. 3a), while $[Zn_2(CH_3\mathbf{L5})(CH_3COO)_2]PF_6$, due to the bulky pendant vinylbenzyl group, needs an excess of substrate to form species with one or two DPP bound. Fig. 3b illustrates how a large excess of DPP changes the species distribution for $[Zn_2(CH_3\mathbf{L5})(CH_3COO)_2]PF_6$, the main species now being $[Zn_2(CH_3\mathbf{L5})(DPP)_2]^+$. These experiments demonstrate that the complexes can bind one or two phosphate substrate molecules readily and show that the acetates are not inhibiting substrate binding.

## NMR spectroscopy

NMR spectra were recorded for both complexes in a range of solvents. Fig. S4 and S5† show a comparison between the free $CH_3H\mathbf{L4}$ ligand and its zinc(II) complex. A low intensity structure, not stemming from free ligand, is present (marked with *). It is possible that these resonances represent either the minor isomer observed in the X-ray crystal structure, or are due to the ether arm not coordinated; a combination of both is possible.

The aliphatic region is shown in Fig. S5† and demonstrates how the protons of the $CH_2$-groups in the free ligand become inequivalent upon zinc binding, in accordance with the lack of a $C_2$-symmetry axis or other symmetric features in the complex. The ratio of low intensity isomer (* in Fig. S4†) to the major isomer depended strongly on the water content in the mixture.

In an experiment where aliquots of $D_2O$ were titrated into a solution of the complex in $CD_3CN$, the proportion of the low intensity species first reduced and then another set of low intensity resonances appeared at higher field (Fig. S6†), highlighting the importance of the medium on species formation and distribution.

To monitor how well $CH_3H\mathbf{L5}$ would assemble a catalytically competent dinuclear Zn(II) centre a $^1$H-NMR titration experiment was conducted. Fig. S7† shows the spectral changes after successive addition of one and two equivalents of zinc(II) acetate to a solution of $CH_3H\mathbf{L5}$ in $CD_3CN$. After each addition the solvent in the NMR tube was brought to

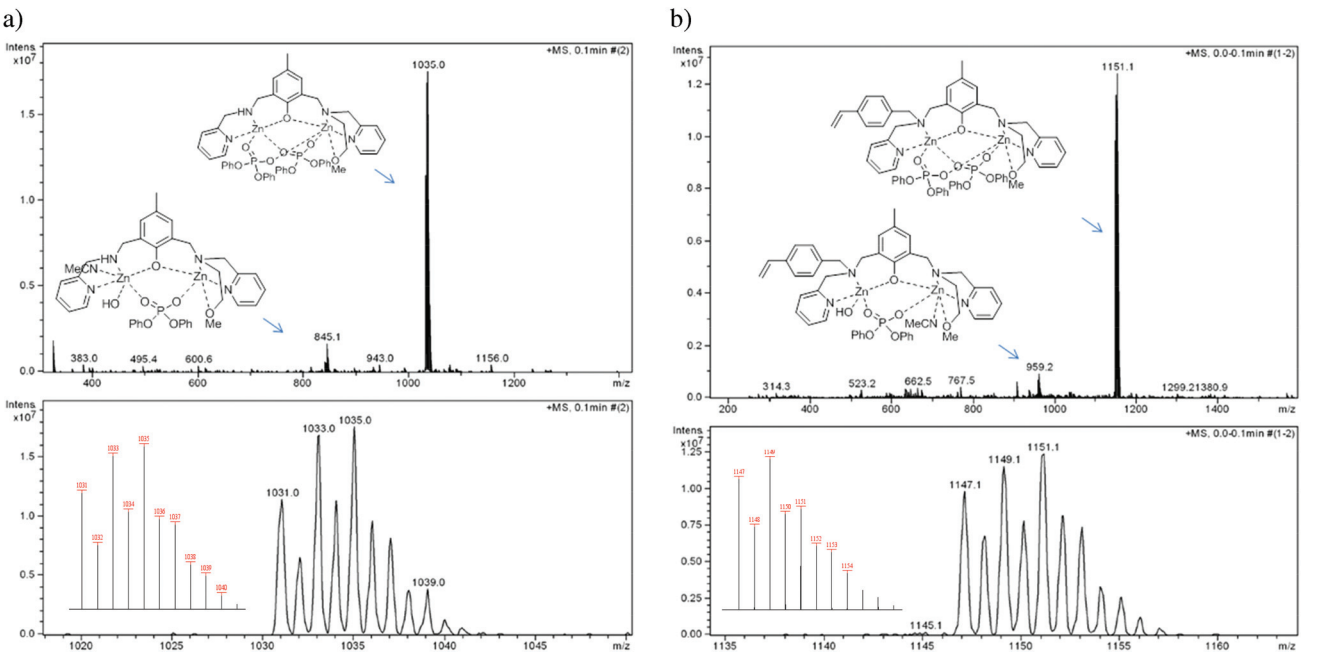


**Fig. 3** (a) Mass spectrum of $[Zn_2(CH_3\mathbf{L4})(CH_3COO)_2]PF_6$ in the presence of excess (>25 eq.) diphenylphosphate in MeCN. Final concentration of complex and substrate were 10 and 250 μM, respectively. (b) Mass spectrum of $[Zn_2(CH_3\mathbf{L5})(CH_3COO)_2]PF_6$ in the presence of excess (>25 eq.) DPP in MeCN. Final concentration of complex and substrate were 10 and 250 μM, respectively.

reflux for 5 minutes prior to spectra recording. After addition of one equivalent of zinc(II) acetate the resonances of the vinyl protons had experienced negligible shifts suggesting that the ligand binds zinc(II) ions in a stepwise manner, occupying first the less sterically hindered site. It is also apparent that after the addition of two equivalents zinc(II) acetate, the solution still contains partially uncomplexed ligand. Addition of another equivalent of zinc(II) acetate resulted in a set of two independent resonances for the vinyl-protons in the spectrum of the fully assembled dinuclear complex, suggesting two isomeric forms in solution. Substrate binding was investigated with $^{31}$P NMR spectroscopy. The addition of one equivalent DPP to a solution of $[Zn_2(CH_3\mathbf{L4})(CH_3COO)_2]PF_6$ in $CD_3CN$ shows multiple phosphate ester species but no resonance from free DPP (expected ~−12 ppm) in accordance with the electrospray mass spectra experiments which showed high affinity for this substrate (Fig. S8a†). In accordance with the mass spectrum of complex having one or two species bound, the different signals observed in the $^{31}$P-spectrum are assigned to a mix of species with one DPP monodentately or bidentately bound (−8.0 and −8.3 ppm), and two DPP molecules also mono- or bidentately bound (−9.1 and −9.5 ppm). Addition of a second equivalent of DPP leads to an increase in intensity of the two resonances at −9.5 and −9.1 ppm (Fig. S8b†), supporting the proposal of two DPP bound to the zinc complex in either a either mono- or bidentate fashion. Further addition of DPP gives rise to a signal at −12.2 ppm attributed to free DPP (Fig. S8c†). In the $^1$H NMR spectrum of $[Zn_2(CH_3\mathbf{L5})(CH_3OO)_2]^+$ with one and two equivalents of substrate (Fig. S9c, d†) the signals are broadened suggesting a bridging DPP conformation.[42] One of the two sets of resonances attributed to the vinyl proton loses intensity upon the addition of one or two DPP molecules to the NMR mixture (Fig. S9c–e†). Given the bulky nature of the vinyl benzyl moiety these results support the notion that in solution the vinyl benzyl group exists in two conformations one directed towards the Zn(II) centre and one pointing in the opposite direction, the latter not being influenced by substrate binding. Moreover, the vinyl benzyl group displays, after the addition of five equivalents DPP (Fig. S9e†), $^1$H-chemical shifts similar to those found in the spectrum of the free ligand (Fig. S9a†). This implies that the vinyl benzyl group points away (and is not further influenced) from the zinc(II) ions when substrate is bound.

When comparing the $^{13}$C NMR spectra of free complex to that in the presence of five equivalents of DPP it is observed that the former spectrum has two sets of vinyl resonances at 114.9 and 115.2 ppm while the latter exhibits only one at 115.2 ppm. Moreover, the carbonyl$_{OAc}$ resonance shifts upon addition of DPP to the complex from 179.0 ppm (bridging acetate) to 173.1 ppm (free acetate).[43] The methyl$_{OAc}$ resonance also exhibits a shift (from 23.1 to 20.8 ppm), suggesting that the acetates remain associated with the complex in solution, but are readily displaced by phosphoester substrates.

The $^{31}$P NMR spectrum of the $[Zn_2(CH_3\mathbf{L5})(CH_3OO)_2]^+$ complex in the presence of one equivalent DPP shows one broad resonance. This resonance possibly arises from multiple species such as monodentately and bidentately bridged ones, as well as free DPP in the mixture (see Gaussian deconvolution in Fig. S10a†). Upon addition of a further equivalent of DPP to the mixture the resonance arising from free DPP becomes more clearly resolved (Fig. S10b†). This resonance becomes the major species upon addition of excess DPP (see spectrum c in Fig. S10†). It should be noted that initially all NMR-titration experiments were conducted in the same solvent mixture as used for the kinetic studies (1 : 1 water–acetonitrile), however, the spectra were in general noisier than in pure acetonitrile which is attributed to the poor solubility of the ligands in the water–acetonitrile mixture. An example titration of zinc acetate and subsequently diphenyl phosphate to the ligand $CH_3H\mathbf{L5}$ in $D_2O$–$CD_3CN$, is included in the ESI (Fig. S11†).

### Immobilisation of $[Zn_2(CH_3\mathbf{L4})(CH_3COO)_2]^+$ on Merrifield resin

M-$CH_3H\mathbf{L4}$ was prepared by reacting the secondary amine group of $CH_3H\mathbf{L4}$ with the chloromethylated Merrifield resin (MR). The dizinc(II) complex was generated subsequently by adding excess zinc acetate to the ligand substituted resin. The IR spectrum (Fig. S12†) of M-$[Zn_2(CH_3H\mathbf{L4})(CH_3COO)_2]^+$ clearly shows the appearance of the two asymmetric and symmetric acetate stretches (marked with *) when compared to the spectrum of unsubstituted MR. Broad absorption bands at 3300 cm$^{-1}$ indicate the presence of OH moieties probably in the form of Zn(II) bound water or methanol. IR bands assigned to symmetric and asymmetric acetate vibrations were not observed when unsubstituted resin was treated with zinc acetate. The XPS of commercially available MR showed, in addition to the expected peaks from carbon and oxygen, the presence of tin oxide;‡ for M-$CH_3H\mathbf{L4}$ peaks attributed to Si 2p electrons were attributed to silicone oil contamination.[44] The XPS of the MR resin treated with $Zn(OAc)_2$ showed only a small amount of zinc (Fig. S13†) and no indication of the presence of nitrogen. The XPS spectra of M-$CH_3H\mathbf{L4}$ showed nitrogen peaks in addition to the peaks from MR (Fig. S13 and S14†). The XPS spectra of M-$[Zn_2(CH_3\mathbf{L4})(CH_3COO)_2]^+$ showed the two peaks typical of Zn 2p electrons (Fig. 4), confirming the uptake of zinc ions. Only one type of nitrogen is resolved, its binding energy typical for tertiary nitrogen (pyridine, tertiary amine).[45,46] A small peak for chlorine (Cl 2p) was found in all spectra (not labelled) and a detailed analysis suggested the presence of both ionic chloride and carbon-bound chloride (Fig. 4). Based on microanalytical data for M-$CH_3H\mathbf{L4}$ and comparison with data for the commercially available resin a catalyst loading of 1.45 mmol g$^{-1}$ was determined.

### Phosphoesterase Activity

The pH dependence of BDNPP hydrolysis was measured from pH 4.75–10 (Fig. 5a). The activity for both $[Zn_2(CH_3\mathbf{L4})(CH_3CO_2)_2]^+$ and $[Zn_2(CH_3\mathbf{L5})(CH_3CO_2)_2]^+$ was dramatically

‡The supplier (Sigma-Aldrich) did not disclose any information whether tin oxide was used in the manufacturing process of this MR so the origin of this contamination is currently unknown.

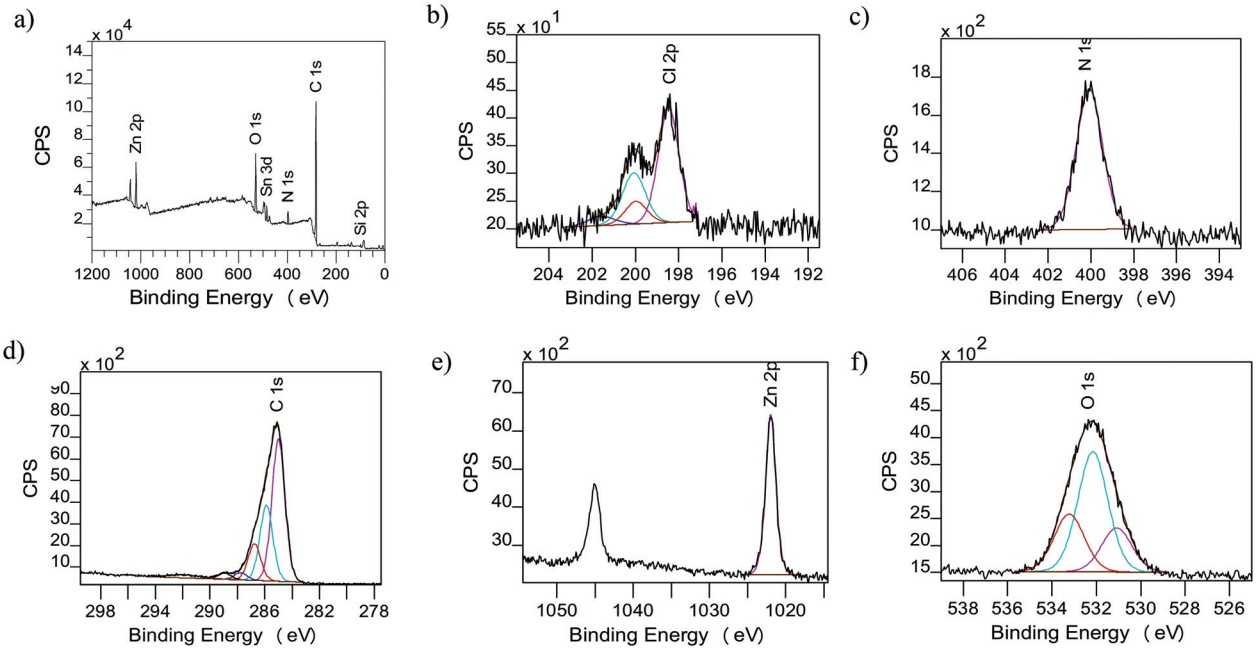


**Fig. 4** (a) XPS survey spectrum of M-$[Zn_2(CH_3\mathbf{L4})(CH_3COO)_2]^+$, Gaussian deconvoluted (b) Cl 2p, (c) N 1s, (d) C 1s, (e) Zn 2p and (f) O 1s spectra of M-$[Zn_2(CH_3\mathbf{L4})(CH_3COO)_2]^+$.

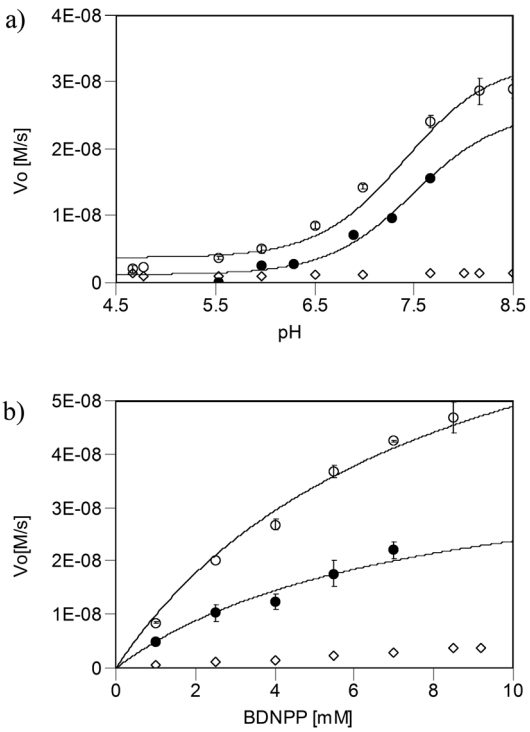


**Fig. 5** (a) pH dependence of the rate of BDNPP hydrolysis by $[Zn_2(CH_3\mathbf{L4})(CH_3COO)_2]^+$ (○) and $[Zn_2(CH_3\mathbf{L5})(CH_3COO)_2]^+$ (●), and (auto)hydrolysis by free Zn(II) (◊). (b) Substrate concentration dependence on the catalytic rate for $[Zn_2(CH_3\mathbf{L4})(CH_3COO)_2]^+$ (○) and $[Zn_2(CH_3\mathbf{L5})(CH_3COO)_2]^+$ (●) and (auto)hydrolysis by free Zn(II) (◊).

reduced above pH 8 and the data became irreproducible; in some cases a white precipitate, presumed to be zinc hydroxide, was observed. The leaching of zinc out of the complex at pH values higher than 8 had been previously reported by Meyer *et al.*[47] The kinetic p$K_a$ values determined for $[Zn_2(CH_3\mathbf{L4})(CH_3COO)_2]^+$ and $[Zn_2(CH_3\mathbf{L5})(CH_3COO)_2]^+$ (7.39 ± 0.19 and 7.50 ± 0.19, respectively) are typical for a zinc-bound water molecule.[29,48] The dependence of BDNPP concentration on the rate of hydrolysis for both complexes (conducted at optimal pH 7.66) followed Michaelis–Menten kinetics (Fig. 5b). The activity of $[Zn_2(CH_3\mathbf{L5})(CH_3COO)_2]^+$ ($k_{cat}$ = 0.97 ± 0.21 × $10^{-3}$ $s^{-1}$, $K_M$ 7.01 ± 2.57 mM; $k_{cat}/K_M$ = 0.14 $s^{-1}$ $mM^{-1}$) is lower than for the less sterically hindered complex $[Zn_2(CH_3\mathbf{L4})(CH_3COO)_2]^+$ ($k_{cat}$ = 2.45 ± 0.27 × $10^{-3}$ $s^{-1}$, $K_M$ = 9.48 ± 1.74 mM; $k_{cat}/K_M$ = 0.26 $s^{-1}$ $M^{-1}$). Compared to $Zn_2$-GpdQ ($k_{cat}/K_M$ = 50 $s^{-1}$ $M^{-1}$)[28] the complexes are ~200 and 360 times less efficient than the enzyme, respectively. The substrate affinity for $[Zn_2(CH_3\mathbf{L4})(CH_3COO)_2]^+$ is slightly higher than for the vinyl benzyl complex, although the error for $K_M$ values is quite large. The phosphoesterase activity of $[Zn_2(CH_3\mathbf{L4})(CH_3CO_2)_2]^+$ appeared typical of that reported for similar types of complexes,[29] suggesting that in this case the asymmetric nature of the ligand has no influence on activity.[1–3] It is clear, however, that the steric bulk engendered by $CH_3H\mathbf{L5}$ does influence the activity.

The phosphatase-like activity of M-$[Zn_2(CH_3H\mathbf{L4})(CH_3COO)_2]^+$ was measured at pH values ranging from 4.75 to 10.5 using BDNPP. The pH dependence of BDNPP hydrolysis for M-$[Zn_2(CH_3\mathbf{L4})(CH_3COO)_2]^+$ is shown (Fig. 6a). The data were consistent with the presence of one protonation equilibrium (p$K_a$ = 7.61 ± 0.71) and were thus fit to an equation derived for a monoprotic system. Above pH 8 the resin leached zinc as was apparent by the presence of a fine white precipitate.[47] Due to the resulting irreproducibility the data above pH

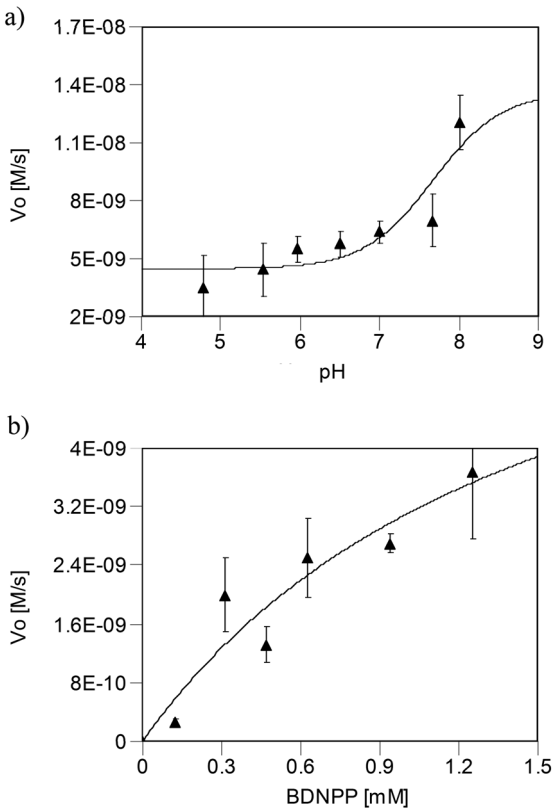


**Fig. 6** (a) pH dependence of BDNPP hydrolysis by M-[$Zn_2(CH_3$**L4**$)(CH_3COO)_2]^+$ (▲), (b) Michaelis–Menten profile for BDNPP hydrolysis by M-[$Zn_2(CH_3$**L4**$)(CH_3COO)_2]^+$ at pH 8.

8 are not displayed. A Michaelis–Menten profile was recorded for this complex at pH 8 with BDNPP, following the same procedure as used for the pH dependence (Fig. 6b). Here, $V_{max}$ = $8 \pm 4 \times 10^{-9}$ M $s^{-1}$ with $K_M = 2 \pm 1$ mM and, based on an estimated catalyst loading of 1.45 mmol $g^{-1}$, $k_{cat} = 11 \pm 6 \times 10^{-6}$ $s^{-1}$.

## Conclusion

The crystal structures of $[Zn_2(CH_3$**L4**$)(CH_3COO)_2]PF_6$ and $[Zn_2(CH_3$**L5**$)(CH_3COO)_2]PF_6$ show one vacant site for coordination of nucleophiles and solvent molecules however, the asymmetric ligand sphere did not appear to have a beneficial effect on catalytic activity. The complex $[Zn_2(CH_3$**L5**$)(CH_3COO)_2]PF_6$ with the more bulky ligand has an impaired substrate affinity as shown by mass spectrometry and $^{31}P$ NMR and the diminished catalytic activity is attributed to steric effects of the vinylbenzyl group. Nevertheless, both complexes are competent mimics of the phosphoesterase enzyme GpdQ. In addition, the complexes are also good structural models for this enzyme. $[Zn_2(CH_3$**L4**$)(CH_3COO)_2]PF_6$ was immobilised on Merrifield (polystyrene) resin and showed activity towards organophosphoester substrate. $[Zn_2(CH_3$**L5**$)(CH_3COO)_2]PF_6$ with the vinyl benzyl arm can be described as the 'monomer' of the immobilised complex. Moreover, the results presented herein suggest that incorporation of these types of complexes onto an insoluble supports, in this case Merrifield resin, results in a system exhibiting phosphoesterase activity. The challenge now is two-fold, (i) to enhance the activity of the biomimetic complexes towards environmentally relevant (organophosphate pesticide) substrates, and (ii) to pursue the immobilisation of active and robust metallohydrolases biomimetics for potential application in bioremediation of environments contaminated with phosphate ester pesticides.

## Acknowledgements

This work was funded by a grant from the Australian Research Council (DP0986613). LJD was funded by IPRS and UQ graduate school scholarships.

## Notes and references

1 H. Carlsson, E. Nordlander and M. Jarenmark, *C. R. Chim.*, 2007, **10**, 433–462.
2 M. Jarenmark, S. Kappen, M. Haukka and E. Nordlander, *Dalton Trans.*, 2008, 993–996.
3 M. Jarenmark, E. Csapo, J. Singh, S. Wockel, E. Farkas, F. Meyer, M. Haukka and E. Nordlander, *Dalton Trans.*, 2010, **39**, 8183–8194.
4 E. Lambert, B. Chabut, S. Chardon-Noblat, A. Deronzier, G. Chottard, A. Bousseksou, J.-P. Tuchagues, J. Laugier, M. Bardet and J.-M. Latour, *J. Am. Chem. Soc.*, 1997, **119**, 9424–9437.
5 M. Lanznaster, A. Neves, A. J. Bortoluzzi, B. Szpoganicz and E. Schwingel, *Inorg. Chem.*, 2002, **41**, 5641–5643.
6 C. Belle, I. Gautier-Luneau, L. Karmazin, J.-L. Pierre, S. Albedyhl, B. Krebs and M. Bonin, *Eur. J. Inorg. Chem.*, 2002, **2002**, 3087–3090.
7 C. Belle, I. Gautier-Luneau, J. L. Pierre, C. Scheer and E. SaintAman, *Inorg. Chem.*, 1996, **35**, 3706–3708.
8 S. Albedyhl, M. T. Averbuch-Pouchot, C. Belle, B. Krebs, J. L. Pierre, E. Saint-Aman and S. Torelli, *Eur. J. Inorg. Chem.*, 2001, **2001**, 1457–1464.
9 S. Albedyhl, D. Schnieders, A. Jancso, T. Gajda and B. Krebs, *Eur. J. Inorg. Chem.*, 2002, **2002**, 1400–1409.
10 J. H. Satcher, M. W. Droege, M. M. Olmstead and A. L. Balch, *Inorg. Chem.*, 2001, **40**, 1454–1458.
11 R. R. Buchholz, M. E. Etienne, A. Dorgelo, R. E. Mirams, S. J. Smith, S. Y. Chow, L. R. Hanton, G. B. Jameson, G. Schenk and L. R. Gahan, *Dalton Trans.*, 2008, 6045–6054.
12 F. Meyer, E. Kaifer, P. Kircher, K. Heinze and H. Pritzkow, *Chem.–Eur. J.*, 1999, **5**, 1617–1630.
13 H. Adams, S. Clunas, D. E. Fenton and D. N. Towers, *J. Chem. Soc., Dalton Trans.*, 2002, 3933–3935.
14 I. A. Koval, D. Pursche, A. F. Stassen, P. Gamez, B. Krebs and J. Reedijk, *Eur. J. Inorg. Chem.*, 2003, **2003**, 1669–1674.

 

15 L. Dubois, R. Caspar, L. Jacquamet, P.-E. Petit, M.-F. Charlot, C. Baffert, M.-N. Collomb, A. Deronzier and J.-M. Latour, *Inorg. Chem.*, 2003, **42**, 4817–4827.
16 L. Dubois, D.-F. Xiang, X.-S. Tan, J. Pécaut, P. Jones, S. Baudron, L. Le Pape, J.-M. Latour, C. Baffert, S. Chardon-Noblat, M.-N. Collomb and A. Deronzier, *Inorg. Chem.*, 2003, **42**, 750–760.
17 C. Piovezan, R. Jovito, A. J. Bortoluzzi, H. n. Terenzi, F. L. Fischer, P. C. Severino, C. T. Pich, G. G. Azzolini, R. A. Peralta, L. M. Rossi and A. Neves, *Inorg. Chem.*, 2010, **49**, 2580–2582.
18 Y. L. M. Zee, L. R. Gahan and G. Schenk, *Aust. J. Chem.*, 2011, **64**, 258–264.
19 J. Yang, P. Li and L. Wang, *Synthesis*, 2011, 1295–1301.
20 K. Li, J. Zhang, Z.-W. Zhang, Y.-Z. Xiang, H.-H. Lin and X.-Q. Yu, *J. Appl. Polym. Sci.*, 2009, **111**, 2485–2492.
21 P. Styring, C. Grindon and C. M. Fisher, *Catal. Lett.*, 2001, **77**, 219–225.
22 Q. H. Xia, H. Q. Ge, C. P. Ye, Z. M. Liu and K. X. Su, *Chem. Rev.*, 2005, **105**, 1603–1662.
23 V. Sciannamea, A. Debuigne, Y. Piette, R. Jerome and C. Detrembleur, *Chem. Commun.*, 2006, **40**, 4180–4182.
24 E. Ghanem, Y. Li, C. Xu and F. M. Raushel, *Biochemistry*, 2007, **46**, 9032–9040.
25 K. S. Hadler, L. R. Gahan, D. L. Ollis and G. Schenk, *J. Inorg. Biochem.*, 2010, **104**, 211–213.
26 F. Ely, K. S. Hadler, L. R. Gahan, L. W. Guddat, D. L. Ollis and G. Schenk, *Biochem. J.*, 2010, **432**, 565–573.
27 K. S. Hadler, N. Mitić, F. Ely, G. R. Hanson, L. R. Gahan, J. A. Larrabee, D. L. Ollis and G. Schenk, *J. Am. Chem. Soc.*, 2009, **131**, 11900–11908.
28 C. J. Jackson, K. S. Hadler, P. D. Carr, A. J. Oakley, S. Yip, G. Schenk and D. L. Ollis, *Acta Crystallogr., Sect. F: Struct. Biol. Cryst. Commun.*, 2008, **64**, 681–685.
29 L. J. Daumann, K. E. Dalle, G. Schenk, R. P. McGeary, P. V. Bernhardt, D. L. Ollis and L. R. Gahan, *Dalton Trans.*, 2012, **41**, 1695–1708.
30 R. A. Peralta, A. J. Bortoluzzi, B. de Souza, R. Jovito, F. R. Xavier, R. A. A. Couto, A. Casellato, F. Nome, A. Dick, L. R. Gahan, G. Schenk, G. R. Hanson, F. C. S. de Paula, E. C. Pereira-Maia, S. d. P. Machado, P. C. Severino, C. Pich, T. Bortolotto, H. Terenzi, E. E. Castellano, A. Neves and M. J. Riley, *Inorg. Chem.*, 2010, **49**, 11421–11438.
31 N. V. Kaminskaia, B. Spingler and S. J. Lippard, *J. Am. Chem. Soc.*, 2000, **122**, 6411–6422.
32 I. H. Segel, *Enzyme Kinetics: Behavior and analysis of rapid equilibrium and steady state enzyme systems*, Wiley-Interscience, New York, 1975.
33 A. Altomare, G. Cascarano, C. Giacovazzo, A. Guagliardi, M. C. Burla, G. Polidori and M. Camalli, *J. Appl. Crystallogr.*, 1994, **27**, 435.
34 G. M. Sheldrick, *Acta Crystallogr., Sect. A: Fundam. Crystallogr.*, 2008, **64**, 112–122.
35 G. M. Sheldrick, *SHELXL97: Program for the refinement of crystal structures*, University of Gottingen, Germany, 1997.
36 L. J. Farrugia, *J. Appl. Crystallogr.*, 1999, **32**, 837–838.
37 G.-C. Sun, Z.-H. He, Z.-J. Li, X.-D. Yuan, Z.-J. Yang, G.-X. Wang, L.-F. Wang and C.-R. Liu, *Molecules*, 2001, **6**, 1001–1005.
38 A. K. Boudalis, R. E. Aston, S. J. Smith, R. E. Mirams, M. J. Riley, G. Schenk, A. G. Blackman, L. R. Hanton and L. R. Gahan, *Dalton Trans.*, 2007, 5132–5139.
39 P. Comba, G. N. DeIuliis, G. A. Lawrance, S. M. Luther, M. Maeder, A. L. Nolan, M. J. Robertson and P. Turner, *Dalton Trans.*, 2003, 2188–2193.
40 L. J. Farrugia, *J. Appl. Crystallogr.*, 1997, **30**, 565.
41 K. Nakamoto, *Infrared and Raman spectra of inorganic and coordination compounds*, Wiley, NY, 1978.
42 K. Selmeczi, C. Michel, A. Milet, I. Gautier-Luneau, C. Philouze, J.-L. Pierre, D. Schnieders, A. Rompel and C. Belle, *Chem.–Eur. J.*, 2007, **13**, 9093–9106.
43 H. E. Gottlieb, V. Kotlyar and A. Nudelman, *J. Org. Chem.*, 1997, **62**, 7512–7515.
44 G. L. Weissler and R. W. Carlson, *Vacuum physics and technology*, Academic Press, New York, 1979.
45 NIST, X-ray Photoelectron Spectroscopy Database, Version 4.1, http://srdata.nist.gov/xps/ Accessed 20.2.13.
46 C. D. Wanger, W. M. Riggs, L. E. Davis, J. F. Moulder and G. E. Muilenberg, *Handbook of X-ray Photoelectron Spectroscopy*, Perkin-Elmer Corp., Physical Electronics Division, Minnesota, USA, 1979.
47 B. Bauer-Siebenlist, F. Meyer, E. Farkas, D. Vidovic, J. A. Cuesta-Seijo, R. Herbst-Irmer and H. Pritzkow, *Inorg. Chem.*, 2004, **43**, 4189–4202.
48 J. Burgess, *Metal ions in solution*, Halsted Press, Chichester, 1978.